for the boundary-layer flow longitudinal to a stationary, constant-radius cylinder. For this flow, the wall shear stress obtained from a local similarity solution of the boundary-layer equations is within 2-5% of the difference-differential solution.

References

[1]Sparrow, E. M., Quack, H. and Boerner, C. J., "Local Nonsimilarity Boundary-Layer Solutions," *AIAA Journal*, Vol. 8, Nov. 1970, pp. 1936-1942.

[2]Seban, R. A. and Bond, R., "Skin Friction and Heat Transfer Characteristics of a Laminar Boundary Layer on a Cylinder in Axial Incompressible Flow," *Journal of the Aeronautical Sciences*, Vol. 8, Oct. 1951, pp. 671-675.

[3]Hartree, D. R. and Womersley, J. R., "A Method for the Numerical or Mechanical Solution of Certain Types of Partial Differential Equations," *Proceedings of the Royal Society of London*, Ser. A, Vol. 101, Aug. 1937, pp. 353-366.

[4]Smith, A. M. O. and Clutter, D. W., "Solution of the Incompressible Laminar Boundary-Layer Equations," *AIAA Journal*, Vol. 1, Sept. 1963, pp. 2062-2071.

[5]Glauert, M. B. and Lighthill, M. J., "The Axisymmetric Boundary Layer on a Long Cylinder," *Proceedings of the Royal Society of London*, Ser. A. Vol. 230, No. 1181, June 1966, pp. 188-203.

[6]Wanous, D. J. and Sparrow, E. M., "Longitudinal Flow Over a Circular Cylinder with Surface Mass Transfer," *AIAA Journal*, Vol. 3, Jan. 1965, pp. 147-149.

Closed-Form Model for Three-Dimensional Vacuum Plumes from a Scarfed Nozzle

G. L. Romine* and J. A. Noble†
Martin Marietta Corporation, Denver, Colorado

Nomenclature

C_F = axial-component thrust coefficient
E = coefficient in density model
F = axial-component thrust parameter
M = Mach number
N = exponent in density model
P = pressure
R = radius from nominal exit plane to point in the plume
T = temperature
V = velocity
α = thrust vector angle from nozzle axis
γ = ratio of specific heats
ζ = polar/azimuthal function used in density model
θ = azimuthal angle from nozzle axis
ν = Prandtl-Meyer angle
ρ = density
σ = scarf angle of exit plane from axis normal
ϕ = polar angle about axis, from highest area ratio

Superscripts

( )* = throat condition

Subscripts

ex = nozzle exit condition
m = condition at expansion to $T = 0$ deg
c = chamber conditions
B = boundary
N = nozzle

Received May 5, 1983.

*Sr. Staff Engineer. Member AIAA.
†Engineer. Member AIAA.

PLUME impingement by attitude control system (ACS) exhausts during deployment or retrieval maneuvers in space can cause serious dispersions to payload trajectories. In order to quantify these ACS plume effects, a reliable model is desired for the plume flowfield. If the ACS nozzle centerline is not perpendicular to the vehicle surface, the exit plane is scarfed or tilted relative to the nozzle axis. The exit Mach number and expansion into the plume will vary peripherally depending upon the local area ratio. Consequently, scarfed nozzle plumes are three dimensional and difficult to quantify. Prior attempts to bound these flows consisted of a patchwork of axisymmetric calculations for each quadrant, and an extrapolation across the axis and between quadrants.

For ease in computation, a closed-form analytical model is desired to simulate the three-dimensional vacuum plume from a scarfed nozzle. A second requirement of the model is that, in the limit of zero scarf angle, the model describes a vacuum plume from a conventional nozzle and takes into account the plume size as a function of maximum turning at the exit. A further requirement for the model is that the exponent for the angular density dependence follow the two-dimensional hypersonic approximation of $2/\gamma - 1$ shown by Boynton[1] to apply to the leading edge of the plume expansion. Although several models are available in the literature for axisymmetric vacuum plumes, none meet the last two requirements directly for the scarfed nozzle plume modifications. The model of Karydas and Kato[2] assumes a fixed 90-deg plume boundary angle, but was the most adaptable for the present requirements and was used as a departure point.

The standard vacuum plume assumptions are made; i.e., the flow can be represented by a source, the density decays with the inverse distance squared, the gas expands to its limiting velocity, the plume is in a vacuum with no boundary shocks, and that the radial density distribution may be described by a single function. The resulting expression for density is

$$\rho = \frac{E}{2}\rho^* \frac{V^*}{V_m}\left(\frac{R^*}{R}\right)^2 \cos^N \zeta \tag{1}$$

where the constants E and N are to be specified by mass and momentum balances shown below, and the parameter ζ is a three-dimensional plume angle from the centerline which is normalized with its local maximum.

The scarfed nozzle plume description must satisfy certain physical boundary conditions. These are as follows.

1) The plume flow will ultimately adjust to the scarfed exit conditions such that the angle where the maximum density occurs is along the thrust vector α. Consequently, the in-

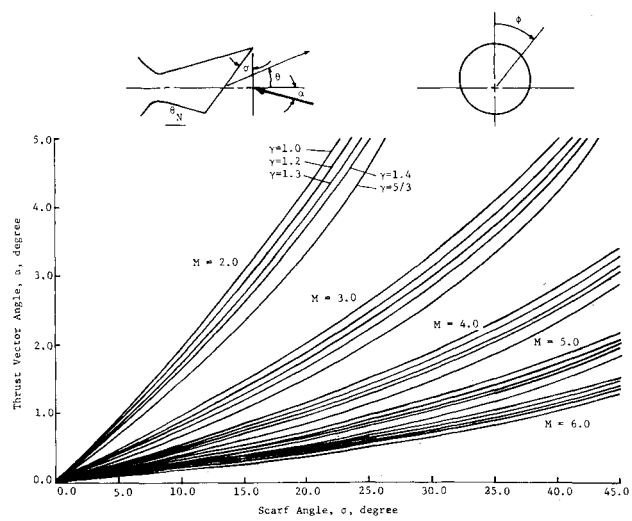

Fig. 1 Thrust vector offset due to scarf angle ($\theta_N = 10$ deg).

tegrated momentum flux through a closed contour is equal to the thrust, and is also directed along α.

2) Streamlines along the nozzle lip at any polar angle ϕ will turn to their local maximum value $\nu_B(\phi)$.

In order to satisfy the first boundary condition, the azimuthal angle θ is modified as $\theta+\alpha\cos\phi$. For the second boundary condition, the azimuthal angle is normalized by $\nu_B(\phi)$ giving the required function as

$$\zeta(\theta,\phi)=\frac{\theta+\alpha\cos\phi}{\nu_B(\phi)+\alpha\cos\phi}\frac{\pi}{2} \tag{2}$$

Without test data, the thrust vector angle α is determined by integrating pressures inside the scarfed nozzle considering it as a truncated cone. The local boundary angle $\nu_B(\phi)$ is a function of the local exit Mach number, the ratio of specific heats γ, and local nozzle half angle $\theta_N(\phi)$, through the relation $\nu_B(\phi)=\nu_m(\phi)-\nu_{ex}(\phi)+\theta_N(\phi)$. The remaining unknowns are the constants E and N which are determined by the conservation of mass and momentum taken over a sphere about the origin.

Mass

$$\pi R^{*2}\rho^* V^* = 2\int_0^{\pi}\int_0^{\nu_B}\rho V_m R^2\sin\theta\,d\theta\,d\phi \tag{3}$$

from which

$$E=\pi\Big/\int_0^{\pi}\int_0^{\nu_B}\sin\theta\cos^N\zeta\,d\theta\,d\phi \tag{4}$$

Axial momentum

$$\pi R^{*2}P_c C_F = 2\int_0^{\pi}\int_0^{\nu_B}\rho V_m^2\cos\theta R^2\sin\theta\,d\theta\,d\phi \tag{5}$$

giving

$$E=\pi F\Big/\int_0^{\pi}\int_0^{\nu_B}\sin\theta\cos\theta\cos^N\zeta\,d\theta\,d\phi \tag{6}$$

where

$$F=\frac{P_c C_F}{\rho^* V^* V_m}=C_F\left(\frac{\gamma+1}{2}\right)^{\frac{1}{\gamma-1}}\left(\frac{\gamma-1}{2\gamma}\right)\left(\frac{\gamma+1}{\gamma-1}\right)^{1/2} \tag{7}$$

Equations (4) and (6) are solved iteratively for E by varying the value of N.

Direct solutions may be obtained for two specific boundary angles and an axisymmetric nozzle (no scarfing). The first is for a plume boundary angle of 180 deg, where the constants E and N are solved for directly,

$$E=\frac{1}{2}\frac{1+F}{1-F},\quad N=4E-2;\quad \sigma=0 \text{ and } \nu_B=\pi$$

The second case is for a plume boundary angle of 90 deg, giving

$$E=\frac{F}{1-F},\quad N=E-1;\quad \sigma=0 \text{ and } \nu_B=\frac{\pi}{2}$$

This last solution was obtained by Karydas and Kato,[2] to apply to any axisymmetric vacuum plume by assuming a fixed 90-deg boundary angle.

The method just given has been used to calculate the flowfield constants for a 10-deg half-angle conical nozzle for several ratios of specific heat and scarf angles. The exit Mach number at the point of maximum expansion within the nozzle was defined as the reference exit Mach number. The results of the parametric study are illustrated in Figs. 1-3. Values of the hypersonic approximation from Boynton are shown at the right of Fig. 3 with general agreement.

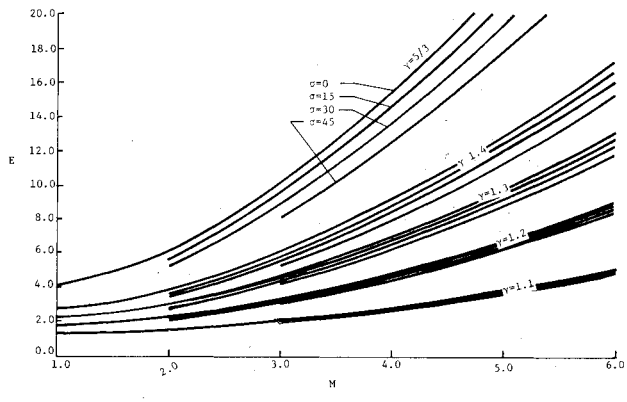

Fig. 2 Parametric study results, parameter E.

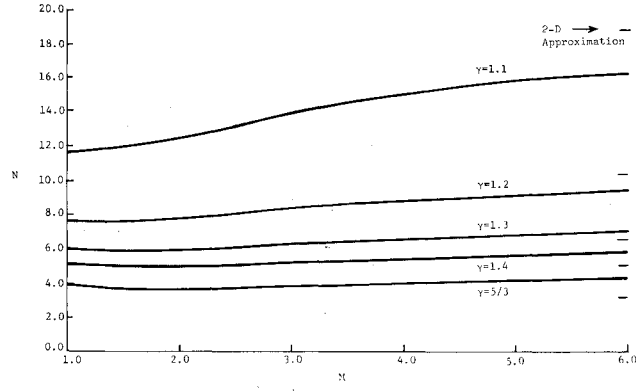

Fig. 3 Parametric study results, parameter N.

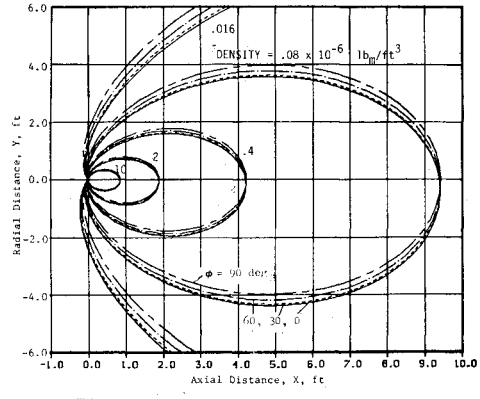

Fig. 4 Constant density contours.

The present method has also been used to calculate the plume flowfield for a typical ACS engine. The engine chosen was modeled as a 10-deg half-angle conical nozzle with a scarf angle of 45 deg, an area ratio of 16, exit radius of 0.1 ft, and chamber conditions of 100 psi, 6000°R, $\gamma=1.2$, and a molecular weight = 20. The plume model for the ACS engine can be expressed in the condensed form

$$\rho=7.1\times10^{-6}\cos^{8.7}\left[\frac{(\theta+4.0\cos\phi)}{\nu_B(\phi)+4.0\cos\phi}90\right](\text{lb/ft}^3)$$

where $\nu_B(\phi)=6.4\cos(\phi+180)+145.4$ is a curve fit to the calculated boundary angle variation with ϕ. Once the constants used in the plume model have been determined, contour plots can be drawn. Figure 4 shows contours of constant density at polar angle cuts in 30-deg increments beginning at 0 deg. The progression for each of the contours clearly shows

the distinct asymmetry at 0 deg, and the gradual approach to symmetry at 90 deg.

In summary, a simple closed-form model has been developed for a three-dimensional vacuum plume from a scarfed nozzle. The model is convenient to use and is adaptable to hand calculators or for onboard algorithms. It is based upon satisfying mass and momentum conservation, while assuming a maximum density along the skewed thrust vector, and an expansion at the nozzle lip based on the local flow conditions around the nozzle periphery. The model can use either analytical or test-determined thrust vector coefficients. For zero scarf angles, the model collapses to an axisymmetric form which is applicable up to the inviscid plume boundary angle.

References

[1] Boynton, F. P., "Highly Underexpanded Jet Structure: Exact and Approximate Calculations," *AIAA Journal*, Vol. 5, Sept. 1967, pp. 1703-1704.

[2] Karydas, A. I. and Kato, H. T., "An Approximate Method for Calculating the Flow Field of a Rocket Exhausting into a Vacuum," Aeronutronics TN No. 24, June 15, 1964.

Singular Propagation Behavior of Cracks in Stiffened Cylindrical Shells

Chang Shangchow*
Northwestern Polytechnical University, Xian, China

Introduction

THIS Note discussed two new findings in crack propagation behavior: namely, the adverse effect of stiffeners on the fracture strength of, and the biased fatigue crack propagation in stiffened cracked cylindrical shells. The former implies that the fracture strength of a stiffened cracked shell can be inferior to that of a similar but unstiffened one under certain conditions, while the latter refers to the sheer unsymmetrical fatigue crack propagation taking place from a symmetrical stiffened cracked shell under symmetrical loading conditions prior to and during the early stage of the crack propagation. These manifestations of crack propagation behavior are all seemingly abnormal and may be called singular. In subsequent sections, we will first describe the phenomenon of singular behavior, together with related testing data. Then an approximate engineering analysis of the stress intensity factors in stiffened cracked shells will be given as evidence that the singular behavior really results from the interaction between stiffeners and cracks in shells. This interaction, in general, is complicated and must be treated carefully in the design of shell-like structural components, such as aircraft pressure cabins, under the concept of damage tolerance.

Testing Data and Phenomena

Singular propagation behavior has been observed during the fracture and fatigue crack propagation tests on stiffened, longitudinally cracked circular cylindrical shell specimens. All of the shells and the circumferential ring-shaped stiffeners were fabricated from 1-mm thick, 2024-T3 aluminum alloy rolled plates. Three types of final specimen configurations are shown in Fig. 1. The stiffeners are attached to the shells' outer surfaces by riveting. Prior to testing, a thorough longitudinal crack symmetrical to the center section of the shell was precracked into each specimen. A uniform, monotonically increasing (or fluctuating) hydraulic pressure was applied on the inner surface of a specimen during fracture (or fatigue crack propagation) testing.

The adverse effect of stiffeners on the fracture strength of cracked shells presented itself in the fracture tests on double-stiffened specimens, as if the crack length is within a definite range, the fracture strength of double-stiffened cracked shells will be inferior rather than superior to that of similar unstiffened shells. This conclusion is supported by the testing evidence of the average value of the burst pressure in fracture tests for double-stiffened specimens having an initial crack of 60 mm in length, 5.66 normal atm, and a higher average value of 6.25 normal atm for similar unstiffened specimens. Also, using the well-known Paris-Foreman law,

$$\frac{da}{dN} = \frac{C_1(\Delta K)^m}{(1-K_{\min}/K_{\max})K_c - \Delta K} \tag{1}$$

the testing data obtained from the fatigue crack propagation tests on various specimens have been processed statistically by the least-squares technique and the final results are $C_1 = 3.31 \times 10^{-12}$, $m = 5.35$ for unstiffened specimens, and $C_1 = 3.98 \times 10^{-12}$, $m = 5.35$ for double-stiffened shell specimens. The data demonstrate clearly that the fatigue crack propagation resistance of double-stiffened specimens is weaker than that of similar unstiffened specimens, in agreement with the results of fracture tests. On these grounds it is recognized that the adverse effect does exist.

The biased fatigue crack propagation behavior was observed in fatigue crack propagation tests on single-stiffened cracked shell specimens. It appeared that during the early stage of fatigue crack growth, two tips of the crack (having a initial length of 40 mm) propagated essentially symmetrically, i.e., both tips gained almost the same crack length increment when a definite number of loading cycles had been carried out. This symmetrical manner of crack propagation appeared normal since, prior to the initiation of fatigue crack growth, all the testing conditions were symmetric to the central stiffener and the external load was a hydraulic pressure (fluctulating between 2-10 normal atm) applied uniformly over the inner surface of the shell. However, whenever the one-sided crack length increment reached about 8 mm, one of the tips ceased growing, while the other one continued its course until the one-sided rapid crack propagation took place. At first it was considered that one might attribute the biased crack propagation to some veiled unsymmetrical factors involved in the testing conditions, and a number of measures had been taken to improve the symmetry of the specimen and loading in the testing procedure. Nevertheless, the biased crack propagation presented itself repeatedly. In addition, similarly biased crack propagation was observed in fracture tests of specimens of the same type. During the initial stage of stable

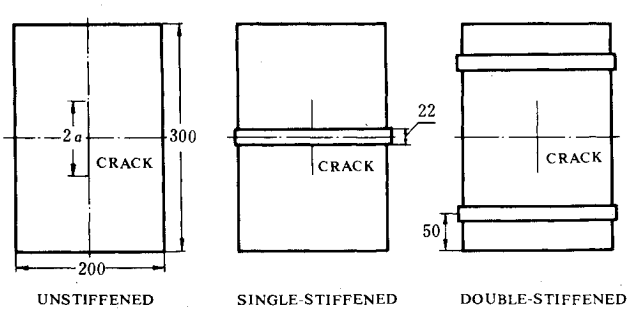

Fig. 1 Specimen configurations (units in millimeters).

Received Dec. 30, 1982; revision received July 11, 1983.

*Associate Professor, Department of Aircraft Engineering.